Electrical Tuning of Single Nitrogen-Vacancy Center Optical Transitions Enhanced by Photoinduced Fields

L. C. Bassett, F. J. Heremans, C. G. Yale, B. B. Buckley, and D. D. Awschalom

Phys. Rev. Lett. **107**, 266403 — Published 22 December 2011

DOI: 10.1103/PhysRevLett.107.266403

Electrical Tuning of Single Nitrogen-Vacancy Center Optical Transitions Enhanced by Photoinduced Fields

L. C. Bassett,* F. J. Heremans,* C. G. Yale,* B. B. Buckley,* and D. D. Awschalom†

Center for Spintronics and Quantum Computation,

University of California, Santa Barbara, CA 93106, USA

Abstract

We demonstrate precise control over the zero-phonon optical transition energies of individual nitrogen-vacancy (NV) centers in diamond by applying multi-axis electric fields, via the DC Stark effect. The Stark shifts display surprising asymmetries that we attribute to an enhancement and rectification of the local electric field by photoionized charge traps in the diamond. Using this effect, we tune the excited state orbitals of strained NV centers to degeneracy and vary the resulting degenerate optical transition frequency by >10 GHz, a scale comparable to the inhomogeneous frequency distribution. This technique will facilitate the integration of NV-center spins within photonic networks.

PACS numbers: 71.55.Cn, 71.70.Ej, 78.56.-a, 81.05.ug

Nitrogen-vacancy (NV) centers in diamond are promising solid-state qubits for emerging quantum technologies, due to their long spin coherence times [1] and fast manipulation rates [2], together with a level structure that allows for straightforward optical initialization and readout of the electronic spin state [3]. Furthermore, in high-quality single-crystal diamond at temperatures below ≈25 K [4], sharp zero-phonon-line (ZPL) optical transitions facilitate the coherent coupling between NV-center spins and photons [5, 6]. The integration of NV centers within photonic structures [7] to route single photons and enhance the spin-photon interaction could therefore lead to scalable applications for quantum information processing and secure communication [8].

As solid-state 'trapped atoms,' NV centers are sensitive to their local environment. While this sensitivity has enabled nanoscale magnetic [9] and electric [10] metrology, it also exposes individual NV centers to sample inhomogeneities, leading to a distribution of ZPL frequencies within a diamond [11]. The ability to tune these frequencies is crucial for photonic applications, for instance to utilize the selection rules at the C_{3v} symmetry point for spin-photon entanglement [6] or to coherently couple distant NV centers to indistinguishable photons. Through the DC Stark effect, applied electric fields perturb both the ground-state spin [10, 12] and excited-state orbitals [13], providing the means to control the optical transitions.

Here we use micron-scale devices to manipulate electric fields in three dimensions, to compensate the intrinsic local strain and electrostatic fields of individual NV centers and achieve full control of the orbital Hamiltonian. Furthermore, by analyzing the Stark shifts as a function of applied voltages, we infer a surprising amplification and rectification of the local electric field, consistent with electrostatic contributions from photoionized charge traps within the diamond host. By harnessing this reproducible effect, we can tune the NV-center Hamiltonian to arbitrary points across a range comparable to the inhomogeneous ZPL distribution.

The electronic structure of the negatively-charged NV center is determined by symmetry, through its point group C_{3v} [11, 14]. The spin-triplet ground (GS, symmetry $^3\mathrm{A}_2$) and excited states (ES, symmetry $^3\mathrm{E}$), are connected by ZPL transitions around 637.2 nm (1.946 eV). Our experiments are performed at zero magnetic field, where the spin-triplet basis states are $\{|S_x\rangle, |S_y\rangle, |S_z\rangle\}$. A 532 nm (2.3 eV) 'repump' beam pulsed at ≈300 kHz in a confocal geometry maintains a spin-polarized population in $|S_z\rangle$. Between repump cycles, we count

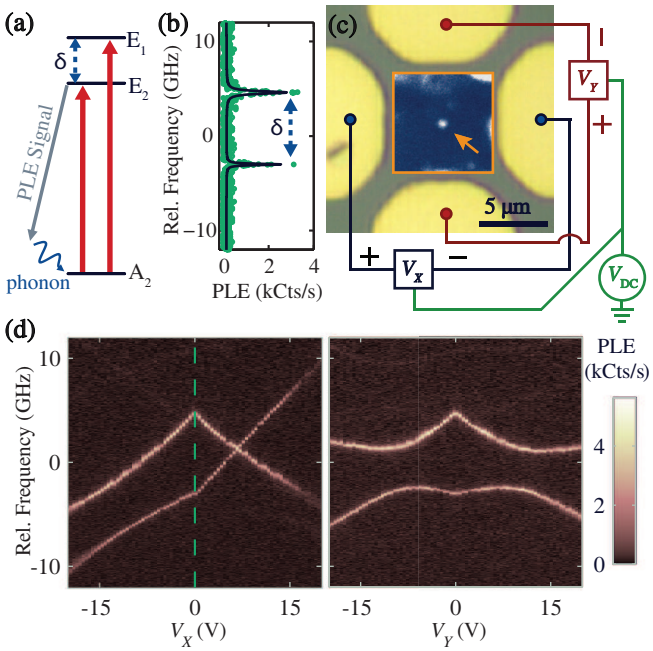

FIG. 1. (a) Simplified energy-level diagram (not to scale) showing only the $|S_z\rangle$ levels of the NV-center ground and excited states, with resonant excitation (red arrows) and red-shifted emission (gray arrow) marked. (b) PLE spectrum (points) with no applied bias, marked by dashed line in (d), with a two-Lorentzian fit (solid curve). (c) Micrograph and photoluminescence image (center) of device A, with electrical connections marked. (d) PLE spectra of the 6 μm-deep NV center marked by an arrow in (c) as a function of lateral bias applied symmetrically to the X (left panel) or Y (right panel) gate pairs, with $V_{\mathrm{DC}} = 0\,\mathrm{V}$. In all PLE spectra, the origin of the relative frequency axis is arbitrary.

photoluminescence excitation (PLE) photons emitted by the NV center into the red-shifted phonon sideband (see Fig. 1a) after absorption from a narrow-line red laser tunable across the ZPL transitions. As we scan the red laser frequency, we typically measure two peaks in the PLE spectrum as shown in Fig. 1b; these correspond to spin-conserving transitions from the GS orbital singlet $|\mathrm{A}_2, S_z\rangle$ to the two ES orbital eigenstates $\{|\mathrm{E}_1, S_z\rangle\,, |\mathrm{E}_2, S_z\rangle\}$. In a crystal environment with perfect C_{3v} symmetry and zero electric and magnetic fields these ES orbital states would be degenerate, but the symmetry is generally broken by local crystal strain and by nonuniform electrostatic charge distributions that generate local electric fields.

The DC Stark perturbation to the Hamiltonian, $\hat{H}_{\mathrm{Stark}} = -\hat{\boldsymbol{\mu}} \cdot \mathbf{F}$, describes the interaction between the local electric field $\mathbf{F}$ and the electric dipole operator $\hat{\boldsymbol{\mu}}$. For fixed stress, the

strain perturbation can be cast into the same form by isolating components which transform as the irreducible representations of C_{3v} [14]. The combined perturbation has the form $V_{\mathrm{A}_1}\hat{O}_{\mathrm{A}_1} + V_{\mathrm{E}_x}\hat{O}_{\mathrm{E}_x} + V_{\mathrm{E}_y}\hat{O}_{\mathrm{E}_y}$, where $\hat{O}_{\Gamma_a}$ is an orbital operator transforming as the basis state $|\Gamma_a\rangle$ and

$$\begin{cases} V_{\mathrm{A}_1} = S_{\mathrm{A}_1} - \mu_\parallel F_z \\ V_{\mathrm{E}_x} = S_{\mathrm{E}_x} - \mu_\perp F_x \\ V_{\mathrm{E}_y} = S_{\mathrm{E}_y} - \mu_\perp F_y \end{cases} \tag{1}$$

are the symmetrized field strengths, in terms of fixed strain components S_{Γ_a}, projections of the local electric field F_i, and the reduced matrix elements of the electric dipole operator $\{\mu_\parallel, \mu_\perp\}$. We choose orbital basis states $\{|\mathrm{E}_x\rangle, |\mathrm{E}_y\rangle\}$ for the ES which transform like vectors $\{x, y\}$ in the NV-center coordinate system [15], and we ignore the small (≈100 MHz) spin-spin coupling between ES spin states $|S_z\rangle$ and $\{|S_x\rangle, |S_y\rangle\}$ [16]. By defining $\hat{H}\,|\mathrm{A}_2, S_z\rangle \equiv 0$, the Hamiltonian in the $\{|\mathrm{E}_x, S_z\rangle, |\mathrm{E}_y, S_z\rangle\}$ basis can be written as

$$H = (\hbar\omega_0 + \Delta\mu_\parallel F_z)\mathbf{I} + \frac{1}{\sqrt{2}} \begin{pmatrix} V_{\mathrm{E}_x} & -V_{\mathrm{E}_y} \\ -V_{\mathrm{E}_y} & -V_{\mathrm{E}_x} \end{pmatrix}, \tag{2}$$

where $\hbar\omega_0$ is the natural transition energy including fixed perturbations of A_1 symmetry, and $\Delta\mu_\parallel = \left(\mu_\parallel^{\mathrm{GS}} - \mu_\parallel^{\mathrm{ES}}\right)$, defined such that both $\Delta\mu_\parallel$ and $\mu_\perp$ are positive. The transition energy eigenvalues take the form $E_\pm = h\bar{\nu} \pm \frac{1}{2}h\delta$, where

$$h\bar{\nu} = \hbar\omega_0 + \Delta\mu_\parallel F_z, \tag{3a}$$

$$h\delta = \sqrt{2}\left(V_{\mathrm{E}_x}^2 + V_{\mathrm{E}_y}^2\right)^{1/2} \tag{3b}$$

are the longitudinal and transverse components due to fields of A_1 and E symmetry, respectively. From Eq. (1), it is clear that a local electric field can cancel the transverse components of intrinsic strain to restore C_{3v} symmetry to the system, and from Eq. (3a) we see that an electric field F_z applied along the NV-center symmetry axis shifts the energy of both transitions by the same amount.

We first investigate these effects using device A, shown in Fig. 1c, consisting of four Ti/Pt/Au gates fabricated on the diamond surface. The sample is a 0.5 mm-thick single-crystal diamond grown by chemical vapor deposition with <5 ppb nitrogen content (ElementSix), irradiated with 2 MeV electrons (1.2×10^{14} cm^{-2}) and then annealed at 800 °C to create NV centers. Measurements are performed in a continuous-flow cryostat operating at

≈20 K. Symmetric biases V_X and V_Y applied as shown in Fig. 1c produce 'lateral' electric fields F_X and F_Y in the [110] and [$\bar{1}$10] crystal directions, respectively, while a common DC bias generates fields in the [001] out-of-plane (Z) direction. The sample (X, Y, Z) and NV-center (x, y, z) coordinate systems are uniquely related for a given NV-center projection from the $\langle 111 \rangle$ family [17].

Figure 1d contains a series of PLE spectra showing the optical resonances of the NV center marked in Fig. 1c, as a function of separate biases V_X and V_Y with $V_{\mathrm{DC}} = 0\,\mathrm{V}$. The lateral biases are applied as symmetrically-pulsed square waves at 1 kHz, with PLE photons binned according to polarity. While the response to static lateral bias is qualitatively similar, this technique separates slow photoinduced charging effects from the dielectric response as discussed below. Two features are evident in the data: first, we observe an unexpected 'kink' at zero bias, and second, the resonances cross at $V_X \approx 7\,\mathrm{V}$, demonstrating that we can indeed restore C_{3v} symmetry to the system. We explore both of these features below with additional experiments.

The kink at zero bias reflects an asymmetry in the local electric field vector as a function of polarity, i.e., $\mathbf{F}(+V) \neq -\mathbf{F}(-V)$. We argue that this asymmetry results from the photoionization of charge traps in the diamond host. Even in high-quality single-crystal synthetic diamonds, deep defects such as vacancy complexes and substitutional nitrogen have important effects on the material's electronic properties [18]. In particular, substitutional nitrogen atoms form donor levels ≈1.7–2.2 eV below the conduction band edge [19], and the timescale for charge transport through these levels is very long (hours) even in nitrogen-rich diamond at room temperature [20]. These traps are easily ionized by the 532 nm repump beam (≈100 μW) which is 4–5 orders of magnitude stronger than the red laser (≈1 nW). When voltages are applied, this leads to a long-lived non-equilibrium charge distribution in the illuminated volume of the sample, which can either amplify or screen the local electric field.

As a simplified one-dimensional demonstration, we present in Fig. 2a the Stark-shift response of an NV center 13 μm below the surface of a second diamond sample irradiated and annealed under similar conditions, but patterned with a global top gate of the transparent conductor indium-tin-oxide (device B). As the top-gate bias is stepped in a loop over ≈160 min, we observe hysteresis in the response characteristic of ≈1 h charge-relaxation timescales. Furthermore, by comparing the magnitudes of the Stark shifts due to biases ap-

plied laterally across an 8 μm gap (Fig. 1d) and vertically across the 0.5 mm sample thickness (Fig. 2a), we find that, when the top-gate bias is negative, the local electric field below the top gate appears to be amplified by roughly an order of magnitude over dielectric predictions [17]; conversely, the field appears to be completely screened above a 'threshold bias,' where the response is flat. The response of an NV center in device A to variations of V_{DC} is qualitatively similar [17], and both are consistent with a picture in which positive charges in the illuminated volume below the NV center rectify the Z-component of the electric field.

We can incorporate these charging effects into a phenomenological model capturing the essential features of our observations. As depicted in Fig. 2b, the local electric field for an NV center between two surface gates is composed of a dielectric component roughly parallel to the sample surface and a rectified component due to photoionized charge that is mainly out of plane. We model this field as

$$\mathbf{F} = \beta V \hat{\mathbf{v}} + \beta |V| \boldsymbol{\xi}, \tag{4}$$

where β accounts for geometric and dielectric factors that predict a local electric field in the direction $\hat{\mathbf{v}}$ in response to an applied voltage V, and $\boldsymbol{\xi}$ is a dimensionless vector giving the relative strength and direction of the rectified field, assumed to scale linearly with $|V|$. Due to the long charging timescale, the rectified field $\beta|V|\boldsymbol{\xi}$ does not change when we switch the bias polarity on millisecond timescales while the dielectric component $\beta V \hat{\mathbf{v}}$ changes sign, producing a polarity-asymmetric response. The assumption of a linear relationship between the rectified field strength and $|V|$ is motivated by the empirical observation that $\bar{\nu}$, proportional to F_z, varies linearly with applied bias in all our measurements. This amounts to an approximation that the spatial distribution of photoionized charge remains fixed, while the charge density varies linearly with $|V|$.

Figure 2c shows the mean ($\bar{\nu}$) and difference (δ) of the transition frequencies extracted from fits to the PLE spectra in Fig. 1d. The NV-center symmetry axis ($[11\bar{1}]$ in this case) is uniquely determined by the sign of $\bar{\nu}$ in response to electric fields in different directions. By substituting Eq. (4) into Eqs. (3) and applying the appropriate coordinate transformation, we obtain a model that quantitatively agrees with our observations [17], as shown by the fits to the data in Fig. 2c. Given that this is only a simplified phenomenological description of a complicated three-dimensional system, it matches our observations surprisingly well.

Finally, we present a control experiment in which we mitigate effects due to the 532 nm

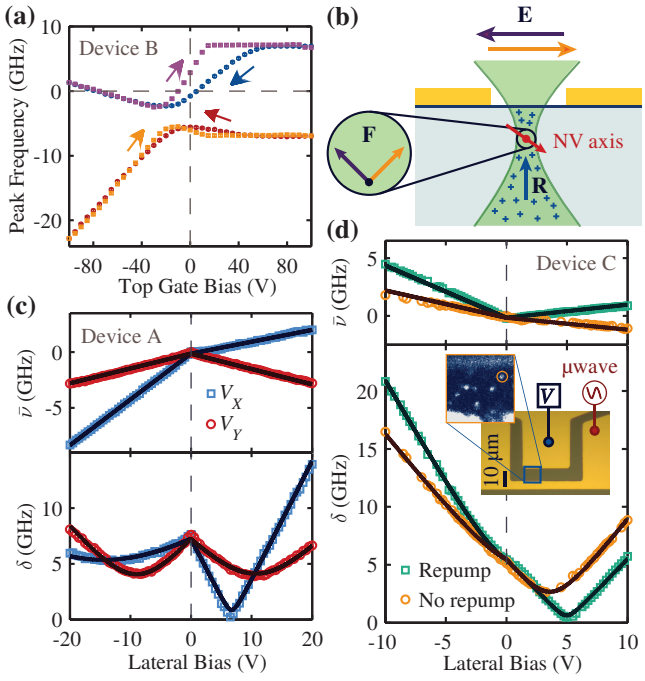

FIG. 2. (a) Stark shift hysteresis loop for an NV center 13 μm below a transparent top gate, as a function of top-gate voltage. Points mark the transition frequencies from a two-Lorentzian fit to a PLE spectrum at the corresponding voltage and color-coded arrows indicate the sweep direction. (b) Schematic of the local electric fields in a lateral geometry. Photoionized charge traps in the illuminated volume contribute a rectified field **R** predominantly in the $+Z$ direction, which adds to the dielectric field **E** to shift the direction of the local field **F**. (c) DC Stark components $\bar{\nu}$ and δ (points) extracted from fits of the PLE spectra in Fig. 1d, with a combined fit according to the model described in the text (solid curves). (d) DC Stark components (points) and fits (solid curves) measured both with (green squares) and without (orange circles) the 532 nm repump excitation. Inset: Micrograph and photoluminescence image of device C, with electrical connections marked. The 7 μm-deep NV center measured in (d) is circled. In all cases, marker sizes slightly exceed measurement uncertainties.

repump cycle. Occasional repump pulses are still required to compensate for photoionization of the NV^- charge state due to sequential two-photon absorption, but with weak (<1 nW) resonant light, the required repump period can be increased to several seconds [4], allowing time to apply bias, record a complete PLE spectrum, and re-zero the bias, all between repump pulses. Since weak spin-nonconserving optical transitions quickly polarize the NV-center spin away from resonance in the absence of the repump cycle, we mix the spin

population by applying a microwave magnetic field resonant with the GS spin transition. We use another device for this purpose (device C), shown in Fig. 2d, which is fabricated on the same diamond as our four-gate lateral device. It consists of a short-terminated waveguide to generate microwave fields and serve as ground, and a gate that when biased produces lateral electric fields across an 8 μm gap.

Figure 2d shows $\bar{\nu}$ and δ as a function of gate voltage for the NV center circled in the inset. Once again the bias polarity is switched at 1 kHz and the PLE photons are binned accordingly. A polarity asymmetry is clearly observed when the repump beam is present, particularly as a kink in $\bar{\nu}$, and it is significantly reduced when the biases are applied in the absence of the repump cycle. Fits to the data using our model [17] are shown as solid curves, from which we find that $|\boldsymbol{\xi}|$ is reduced from 0.71±0.02 with the standard repump cycle to 0.33±0.03 when the 532 nm beam is omitted.

Based on this understanding, we can exploit the photoinduced charge to obtain greatly enhanced tunability in our four-gate geometry (device A). Since the rectified field points predominantly out of plane and has strength comparable to the dielectric component, we effectively obtain three-dimensional control of the local electric field vector. The application of a negative reference bias V_{DC} as shown in Fig. 1c increases the rectified component F_Z independently of (F_X, F_Y). As a demonstration of the flexibility of this technique, we present a tuning diagram in Fig. 3 in which we use (V_X, V_Y) to scan through the C_{3v} degeneracy point at different settings of V_{DC}. Each crossing occurs at a different frequency, with the corresponding bias point $(V_X, V_Y, V_{\mathrm{DC}})$ marked in the upper panel. Essentially, we are compensating the transverse components $(S_{\mathrm{E}_x}, S_{\mathrm{E}_y})$ of the intrinsic fields and tuning the longitudinal component of $\mathbf{F}$ to shift the frequency. Since the rectified field always points along $+Z$, we can only tune the frequency in one direction, but the effect is strong enough to produce a >10 GHz shift in the degenerate frequency with practical applied voltages.

With this technique we can tune multiple NV centers to have the same degenerate transition frequency. The PLE spectra outlined in blue in Fig. 3 were obtained from a second NV center in the same device at $V_{\mathrm{DC}} = 0$ V, and display C_{3v} degeneracy at a frequency within the tuning range of the first. If these two NV centers were in separately-controlled devices and tuned simultaneously to degeneracy at the same frequency, they would couple identically to indistinguishable photons.

In conclusion, we have used electric fields to tune the ZPL transitions of individual NV

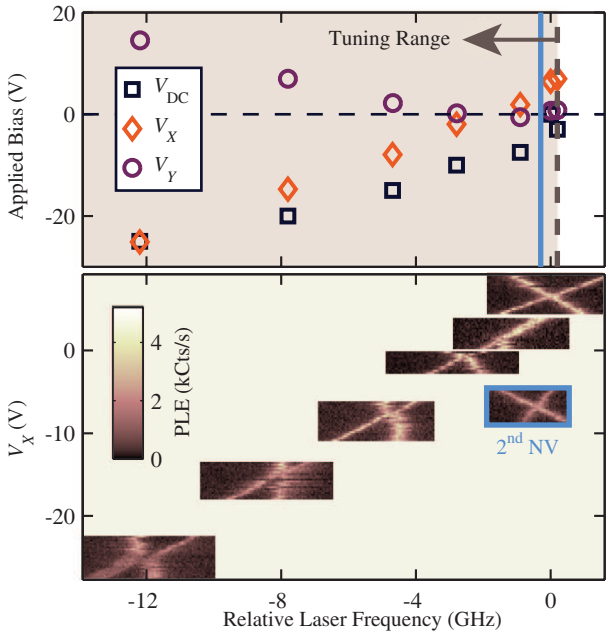

FIG. 3. Tuning diagram for the NV center marked in Fig. 1c. Degeneracy is achieved at different frequencies by setting the applied biases $(V_{\rm DC}, V_X, V_Y)$ as marked in the upper panel; in the lower panel we show PLE spectra as a function of V_X around each of these points for fixed $V_{\rm DC}$ (V_Y is also varied to keep the ratio V_X/V_Y constant). We can shift a second NV center to degeneracy within the tuning range of the first, as shown by the PLE spectra outlined in blue (lower panel) and the corresponding blue line (upper panel) marking the degenerate frequency.

centers in micron-scale devices size-compatible with photonic structures. Through their DC Stark shifts, NV centers serve as nanoscale probes of their electrostatic environment, revealing strong signatures of charge accumulation due to photoionization of deep donor levels in the diamond. We have analyzed these effects with a phenomenological model and used the additional fields provided by photoionization to obtain three-dimensional control of the local electric field, in order to tune both the overall energy and orbital splitting of the excited-state Hamiltonian. In particular, we have demonstrated how to reach the C_{3v} symmetry point and then apply longitudinal perturbations to shift the degenerate photon energy. By coupling multiple NV centers to indistinguishable photons with this technique, photonic networks could provide a quantum bus to coherently couple distant NV centers, and entanglement swapping protocols [8] could enable long-distance quantum key distribution.

We acknowledge financial support from the AFOSR, ARO, and DARPA, and thank R.

Hanson, C. G. Van de Walle, U. K. Mishra, K. Ohno, and D. J. Christle for useful discussions.

---

* These authors contributed equally to this work

† Corresponding author.

Email address: awsch@physics.ucsb.edu

[1] G. Balasubramanian *et al.*, Nat. Mater. **8**, 383 (2009).

[2] G. D. Fuchs *et al.*, Science **326**, 1520 (2009).

[3] N. B. Manson, J. P. Harrison, and M. J. Sellars, Phys. Rev. B **74**, 104303 (2006).

[4] K.-M. C. Fu *et al.*, Phys. Rev. Lett. **103**, 256404 (2009).

[5] B. B. Buckley, G. D. Fuchs, L. C. Bassett, and D. D. Awschalom, Science **330**, 1212 (2010).

[6] E. Togan *et al.*, Nature **466**, 730 (2010).

[7] A. Faraon *et al.*, Nat. Photon. **5**, 301 (2011); C. Santori *et al.*, Nanotechnology **21**, 274008 (2010).

[8] S. D. Barrett and P. Kok, Phys. Rev. A **71**, 060310 (2005); L. Childress, J. M. Taylor, A. S. Sørensen, and M. D. Lukin, *ibid.* **72**, 052330 (2005).

[9] J. R. Maze *et al.*, Nature **455**, 644 (2008); G. Balasubramanian *et al.*, *ibid.* **455**, 648 (2008); B. J. Maertz *et al.*, Appl. Phys. Lett. **96**, 092504 (2010).

[10] F. Dolde *et al.*, Nat. Phys. **7**, 459 (2011).

[11] A. Batalov *et al.*, Phys. Rev. Lett. **102**, 195506 (2009).

[12] E. Van Oort and M. Glasbeek, Chem. Phys. Lett. **168**, 529 (1990).

[13] P. Tamarat *et al.*, Phys. Rev. Lett. **97**, 083002 (2006); New J. Phys. **10**, 045004 (2008).

[14] M. W. Doherty, N. B. Manson, P. Delaney, and L. C. L. Hollenberg, New J. Phys. **13**, 025019 (2011); J. R. Maze *et al.*, **13**, 025025 (2011).

[15] The NV-center coordinate system is chosen such that $\hat{z}$ points along the N-V symmetry axis and $\hat{x}$ lies in a reflection plane.

[16] Note that while spin-spin coupling leads to mixed ES spin eigenstates in some regimes, it does not significantly affect the optical pumping mechanism which polarizes the spin into $|S_z\rangle$ in our experiments.

[17] See supporting online material.

[18] J. Isberg, A. Tajani, and D. J. Twitchen, Phys. Rev. B **73**, 245207 (2006).

[19] R. G. Farrer, Solid State Commun. **7**, 685 (1969); J. Rosa, M. Vaněček, M. Nesládek, and L. M. Stals, Diam. Relat. Mater. **8**, 721 (1999).

[20] F. J. Heremans *et al.*, Appl. Phys. Lett. **94**, 152102 (2009).